BRAIN COMMUNICATIONS

Abnormal brain state distribution and network connectivity in a *SYNGAP1* rat model

Ingrid Buller-Peralta,[1,*] Jorge Maicas-Royo,[1,*] Zhuoen Lu,[2,*] Sally M. Till,[1] Emma R. Wood,[1] Peter C. Kind,[1] Javier Escudero[2] and Alfredo Gonzalez-Sulser[1]

* These authors contributed equally to this work.

Mutations in the *SYNGAP1* gene are one of the common predictors of neurodevelopmental disorders, commonly resulting in individuals developing autism, intellectual disability, epilepsy, and sleep deficits. EEG recordings in neurodevelopmental disorders show potential to identify clinically translatable biomarkers to both diagnose and track the progress of novel therapeutic strategies, as well as providing insight into underlying pathological mechanisms. In a rat model of *SYNGAP1* haploinsufficiency in which the exons encoding the calcium/lipid binding and GTPase-activating protein domains have been deleted ($Syngap^{+/\Delta-GAP}$), we analysed the duration and occurrence of wake, non-rapid eye movement and rapid eye movement brain states during 6 h multi-electrode EEG recordings. We find that although $Syngap^{+/\Delta-GAP}$ animals spend an equivalent percent time in wake and sleep states, they have an abnormal brain state distribution as the number of wake and non-rapid eye movement bouts are reduced and there is an increase in the average duration of both wake and non-rapid eye movement epochs. We perform connectivity analysis by calculating the average imaginary coherence between electrode pairs at varying distance thresholds during these states. In group averages from pairs of electrodes at short distances from each other, a clear reduction in connectivity during non-rapid eye movement is present between 11.5 Hz and 29.5 Hz, a frequency range that overlaps with sleep spindles, oscillatory phenomena thought to be important for normal brain function and memory consolidation. Sleep abnormalities were mostly uncorrelated to the electrophysiological signature of absence seizures, spike and wave discharges, as was the imaginary coherence deficit. Sleep spindles occurrence, amplitude, power and spread across multiple electrodes were not reduced in $Syngap^{+/\Delta-GAP}$ rats, with only a small decrease in duration detected. Nonetheless, by analysing the dynamic imaginary coherence during sleep spindles, we found a reduction in high-connectivity instances between short-distance electrode pairs. Finally comparing the dynamic imaginary coherence during sleep spindles between individual electrode pairs, we identified a group of channels over the right somatosensory, association and visual cortices that have a significant reduction in connectivity during sleep spindles in mutant animals. This matched a significant reduction in connectivity during spindles when averaged regional comparisons were made. These data suggest that $Syngap^{+/\Delta-GAP}$ rats have altered brain state dynamics and EEG connectivity, which may have clinical relevance for *SYNGAP1* haploinsufficiency in humans.

1 Simons Initiative for the Developing Brain, Patrick Wild Centre, Centre for Discovery Brain Sciences, University of Edinburgh, EH8 9XD Edinburgh, United Kingdom
2 School of Engineering, Institute for Digital Communications, University of Edinburgh, EH9 3JL Edinburgh, United Kingdom

Correspondence to: Alfredo Gonzalez-Sulser
Simons Initiative for the Developing Brain Fellow
University of Edinburgh, Centre for Discovery Brain Sciences
1 George Square, Edinburgh, EH89JZ, United Kingdom
E-mail: agonzal2@ed.ac.uk

Keywords: *SYNGAP1*; EEG; connectivity; epileptic encephalopathy; sleep

Received February 04, 2022. Revised July 09, 2022. Accepted October 13, 2022. Advance access publication October 15, 2022

Abbreviations: C2 = calcium/lipid binding; GAP = GTPase activating; NDD = neurodevelopmental disorders; NREM = non-rapid eye movement sleep; REM = rapid eye movement sleep; SWD = spike and wave discharges

Graphical Abstract

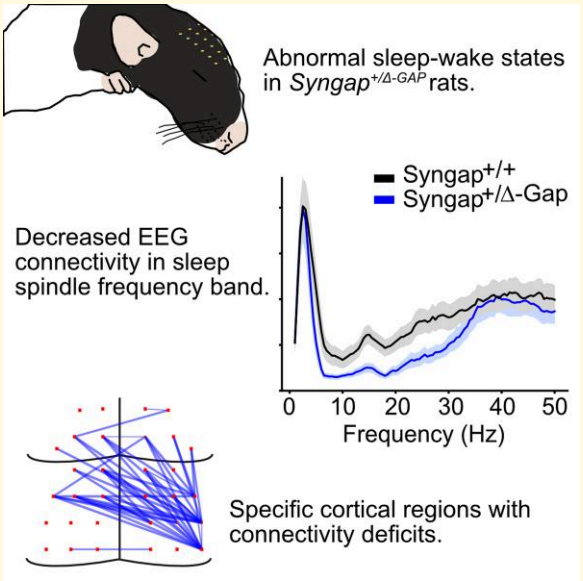

Introduction

Neurodevelopmental disorders (NDDs) encompass multiple disease phenotypes that are linked to a highly heterogenous genetic architecture.[1] Mutations in the *SYNGAP1* gene account for as many as 1% of NDD cases, with patients often presenting with intellectual disability and autism spectrum disorder.[2–6] Most patients with *SYNGAP1* pathogenic variants display some form of epilepsy with a high prevalence of absence seizures and a behavioural developmental delay occurring upon seizure onset. Therefore, *SYNGAP1* haploinsufficiency is often classed as an epileptic encephalopathy.[3,7,8] Additionally, sleep impairments have been reported by parents[3] and have been documented in the clinical setting in a high proportion of cases.[8,9]

Characterization of novel biomarkers of NDDs may allow for early diagnosis and rapid therapeutic intervention, enabling quantitative monitoring of treatment efficacy, which is likely critical for the success of future clinical trials.[10] EEG recordings are a potentially reliable method of identifying biomarkers as they provide a fast and direct measure of overall brain activity.[11] However, given the heterogeneity of aetiologies, phenotypes and disease trajectories of NDDs, biomarkers specific for particular genetic disorders such as *SYNGAP1* are imperative to differentiate between NDD types and identify likely disease outcomes.[12]

The rare incidence of NDD patients with specific mutations makes performing large-cohort EEG studies to identify biomarkers difficult. *SYNGAP1* haploinsufficiency cases are thought to occur in only 6.1 per 100 000 people.[13] Identifying clinically relevant biomarkers in genetically modified rodent models of NDDs is a plausible alternative strategy. Furthermore, these biomarkers may then converge and be applicable to other NDD types.

SYNGAP1 encodes a Ras-GTPase-activating protein, which is mainly expressed in the synapses of excitatory neurons.[14,15] It is a key regulator of the postsynaptic density, synaptic development and plasticity.[16] We recently reported on a novel rat model of *SYNGAP1* haploinsufficiency in which the calcium/lipid binding (C2) and GTPase-activating (GAP) domains, that are thought to be critical for the normal function of *SYNGAP1*, have been deleted.[17] Animals heterozygous for the C2/GAP domain deletion ($Syngap^{+/\Delta-GAP}$) displayed reduced exploration and fear extinction, altered social behaviour and spontaneous absence seizures. SYNGAP plays a critical role in synaptic transmission and organisation, therefore we hypothesize that $Syngap^{+/\Delta-GAP}$ animals have abnormal functional connectivity between different cortical regions during specific brain states.

To record seizures, we previously performed 6-hr recordings utilizing skull-surface 32-channel EEG grids, as these mimic human high-density EEG recordings.[18] Here, we perform detailed analysis of the occurrence of multiple brain states during those recordings and, find abnormalities in $Syngap^{+/\Delta-GAP}$ rats in the duration and number of sleep and wake occurrences during recordings, as well as differences in connectivity between cortical regions that may have value as clinically translatable biomarkers.

Materials and methods

Animals

This paper uses data gathered during experiments for which some results have been previously published.[17] All animal procedures were undertaken in accordance with the University of Edinburgh animal welfare committee regulations and were performed under a United Kingdom Home Office project license. Long Evans-SG$^{em2/PWC}$, hereafter referred to as *Syngap*$^{+/\Delta-GAP}$ were kept on a 12 h/12 h light–dark cycle with ad libitum access to water and food. Animals were genotyped by polymerase chain reaction. 12 *Syngap*$^{+/\Delta-GAP}$ and 12 *Syngap*$^{+/+}$ male animals were recorded and used across all analyses.

Surgery

Fifteen- to 16-week-old *Syngap*$^{+/\Delta-GAP}$ and *Syngap*$^{+/+}$ male rates were anaesthetized with isoflurane and mounted on a stereotaxic frame. Two craniotomies were drilled for bilateral anchor screw placement (+4.0 mm AP, ±0.5 mm ML) and one for ground screw implantation (−11.5 mm AP, 0.5 mm ML) (A2 Din M1 × 3 cheese head screw, Screwsandmore, UK), according to the frontal and caudal edges of the EEG array probe (H32-EEG—NeuroNexus, USA). The EEG probe was placed on the skull with its cross-symbol reference point aligned over bregma (Supplementary Figure 1). The ground electrode and screw were connected with silver paint, and the implant was covered with dental cement. Animals were allowed to recover for a minimum of 1-week post-surgery and were housed individually after surgery to prevent damage to the implant. Animals were monitored for any welfare issues arising during or after surgery, as well as changes in behaviour, such as less food consumption or decreased responses to stimuli in cages, none were found.

EEG recordings

Prior to recording, rats were habituated for 20–30 min to the room. On recording days, up to four rats, were placed in individual side-by-side cages inside a 1 × 1 m faraday enclosure. Experimenters were blind to genotype. Six hour EEG recordings, starting at zeitgeber time (ZT) 3 to 9 (under a 12 light hr:12 dark hr schedule starting at 07:00 am) were acquired with an OpenEphys acquisition system (OpenEphys, Portugal), through individual 32-channel recording headstage amplifiers with accelerometers (RHD2132 Intantech, USA), at a sampling rate of 1 kHz.

Visual sleep scoring and absence seizure detection

Offline visual brain state scoring blind to animal genotype was performed, assigning 5 s epochs to non-rapid eye movement sleep (NREM), rapid eye movement sleep (REM) or wake. Scoring criteria for visual classification was based on accelerometer and EEG characteristics:[19,20] NREM epochs displayed high-amplitude slow-wave (~1–4 Hz) EEG activity accompanied by sleep spindles (~12–17 Hz) and decreased accelerometer activity. REM was identified by sustained theta (~5–10 Hz) and no accelerometer activity. Wake was identified by the presence of desynchronized EEG and varying levels of accelerometer activity.

We validated our accelerometer and EEG-based visual scoring by comparing with recordings performed with electromyogram (EMG) and EEG. 4 *Syngap*$^{+/\Delta-GAP}$ and 4 *Syngap*$^{+/+}$ animals were surgically implanted with a 16-channel EEG surface probe array with two EMG leads (H16-Rat EEG16_Functional—NeuroNexus, MI, USA) implanted in neck muscles. Animals were recorded over 5 days for 24 hr utilizing wireless amplifiers (Tainitec, UK).[21] Visual analysis was performed as described above utilizing EEG combined with EMG instead of accelerometer data over the 6 h recorded in equivalent EEG accelerometer experiments at ZT 3 to 9 (under a 12 light hr:12 dark hr schedule starting at 07:00 am). When comparing EEG–accelerometer and EEG–EMG modalities, we found no significant difference in percent time spent in wake (two-way ANOVA, $F = 0.004$, $df = 1$, $P = 0.95$, $n = 12$ *Syngap*$^{+/\Delta-GAP}$ and *Syngap*$^{+/+}$ EEG–accelerometer and $n = 4$ *Syngap*$^{+/\Delta-GAP}$ and *Syngap*$^{+/+}$ EEG–EMG, Supplementary Figure 2A), NREM (two-way ANOVA, $F = 0.079$, $df = 1$, $P = 0.472$, $n = 12$ *Syngap*$^{+/\Delta-GAP}$ and *Syngap*$^{+/+}$ EEG–accelerometer and $n = 4$ *Syngap*$^{+/\Delta-GAP}$ and *Syngap*$^{+/+}$ EEG–EMG, Supplementary Figure 2B) and REM (two-way ANOVA, $F = 0.531$, $df = 1$, $P = 0.472$, $n = 12$ *Syngap*$^{+/\Delta-GAP}$ and *Syngap*$^{+/+}$ EEG–accelerometer and $n = 4$ *Syngap*$^{+/\Delta-GAP}$ and *Syngap*$^{+/+}$ EEG–EMG, Supplementary Figure 2C).

We previously quantified and reported the occurrence of absence seizures in *Syngap*$^{+/\Delta-GAP}$ rats[17] and excluded their occurrence times from our brain state analyses. The electrographical correlate of absence seizures, spike and wave discharges (SWDs), were identified visually and analysis was confirmed with an automated absence seizure detection algorithm. Briefly, SWDs are characterized by periodic high-amplitude oscillations in the theta band between 5 and 10 Hz[22] which correlates with a spontaneous stop in animal movement. Spectral analysis was performed that identified harmonic peaks in the power spectral density. The code used for analysis is available at https://github.com/Gonzalez-Sulser-Team/SWD-Automatic-Identification.

Automatic detection of sleep spindles

Automatic detection of sleep spindles during visually scored NREM sleep epochs was performed using the Matlab 'Sleepwalker' toolbox with the 'sw_run_delta_LFP.m' function (https://gitlab.com/ubartsch/sleepwalker).[23] EEG signals from the electrode placed over S1-Tr right were band-passed filtered between 12 and 17 Hz, with a minimum–maximum length between 0.2 and 3 s, a minimal time gap between events of 0.2 s, amplitude between 25 and 750 μV, a start to end limit threshold of 1.5 SD with a

detection limit of 3 SD of the envelope, and noise exclusion at ≥ 35 SD.

To detect spindles detected in multiple sites during NREM periods from electrodes that were less than 2 mm away from each other, we used the Python 'Yasa' library function 'spindles_detect' (https://zenodo.org/record/4632409) to identify spindles with a frequency range of 12–17 Hz. The comparison was made specifically in electrodes that were within 2 mm distances from each other.

Spectral power and imaginary coherence analysis

Analysis scripts are available at https://github.com/Gonzalez–Sulser. Movement artefacts, identified visually as data points with values greater than 750 μV were discarded from further analyses. Spectral power for each individual epoch for all brain states (wake, NREM and REM) was calculated from an individual channel over the right primary somatosensory as the mean $\log_{10}$ power in the 0.2–48 Hz range (0.2 Hz steps) using the Multitaper package (Rahim, Burr & Thomson., 2014[5]) for R-studio (RStudio Team, 2020[6]). Epochs were then averaged per brain states for each individual animal.

For imaginary coherence averages across electrode pairs, the data were downsampled by a factor of 8 with the Python 'Scipy.signal' function 'decimate', which includes an order 8 Chebyshev Type I filter for anti-aliasing, to increase processing speed. We calculated the coherence for each of the 32 pairs of electrodes in individual brains states in 99 frequency bins (1–50 Hz, 0.5 Hz bin size) with the Python Scipy 'signal' function 'coherence' and extracted the imaginary component using the Python Numpy function 'imag'.[24] To ensure statistical normality, coherence values (R^2) from each 0.5 Hz frequency were z-transformed using Fisher's r to z, z-scores were then averaged at every 0.5 Hz bin and re-transformed utilizing the Fisher inverse function to obtain the Z^{-1} coherence value per electrode pair and frequency band.[25]

We calculated the Euclidean distance between all pairs of electrode using the Python SciPy 'Spatial.distance' function 'pdist', with 1.3 mm being the shortest distance between adjacent electrodes and 13.9 mm the longest distance electrode leads. We then utilized varying distance thresholds (from 2–10 mm in 1 mm increments) to compare imaginary coherence averages from short and long distances electrode pairs, between the groups of *Syngap*$^{+/\Delta-GAP}$ and *Syngap*$^{+/+}$ animals.[25]

Imaginary phase coherograms, representations of functional connectivity that depend on both frequency and time and are similar to spectrograms, were constructed during spindles using a complex Morlet wave convolution for 12–17 Hz using the 'freqanalysis' function with the 'wavelet' method from the Matlab Fieldtrip package. The wavelet cycle width was set to 7 with a length defined as 3 SDs of the implicit Gaussian kernel. Connectivity analysis utilizing coherograms was performed using the 'connectivityanalysis' function from the Matlab Fieldtrip package. Coherograms were averaged across specified channels over spindle occurrence times (500 ms preceding and 1500 ms following spindle start). Maximal imaginary coherence was identified over all coherogram time–frequency bins, 11 frequency components with 0.5 Hz steps from 12 to 17 Hz over 2000 time points for the 2000ms was analysed, and used to quantify the number of time–frequency bins exceeding 70% of the maximum imaginary coherence.

Statistical analysis

When normality and homoscedasticity were above the rejection value of < 0.05 (estimated by Shapiro–Wilk and Levene's tests, respectively), between genotype comparisons across animals and electrodes were performed with two-sample unpaired t-tests. Otherwise, a two-sample Mann–Whitney U rank sum test was used for unpaired two-sample comparisons. Two-way ANOVAs were utilized to compare EEG–accelerometer with EEG–EMG brain state visual analyses, brain state power spectra and average Z' imaginary coherence in commonly used frequency bands. We performed a non-parametric two-sided permutation analysis with 40 000 simulation runs to compare average coherence per frequency band, and frequency over time during sleep spindles across electrode pairs. Consecutive significant frequencies clusters determined ranges with significant differences.[26] Pearson correlation was used to test the relationship of SWDs with brain state abnormalities and imaginary coherence differences. In this study, we analysed data recorded from *Syngap*$^{+/\Delta-GAP}$ and *Syngap*$^{+/+}$, which previously allowed us to show significant differences in the incidence and duration of absence seizures.[17] For our a priori statistical power calculations for the present study, we utilized an alpha value of 0.05. For comparisons between genotypes of percent time, total minutes and average duration of individual brain state bouts, we estimated animal numbers based on similar results from changes in brain states in mutant mice in another neurodevelopmental model.[27] For total minutes, we set the mean of the control to 75 min, the mean of the mutant group to 55 min and the standard deviation for the mutants was set at 15.8. An $n = 12$ resulted from power set to 0.803 and an effect size of 1.27 (G*Power, Germany).

Data availability

Data can be obtained directly from the corresponding author.

Results

Sleep–wake distribution and spectral properties in *syngap*$^{+/\delta-GAP}$ rats

We previously reported that Syngap$^{+/\Delta-GAP}$ rats displayed absence seizures more frequently than littermate controls,

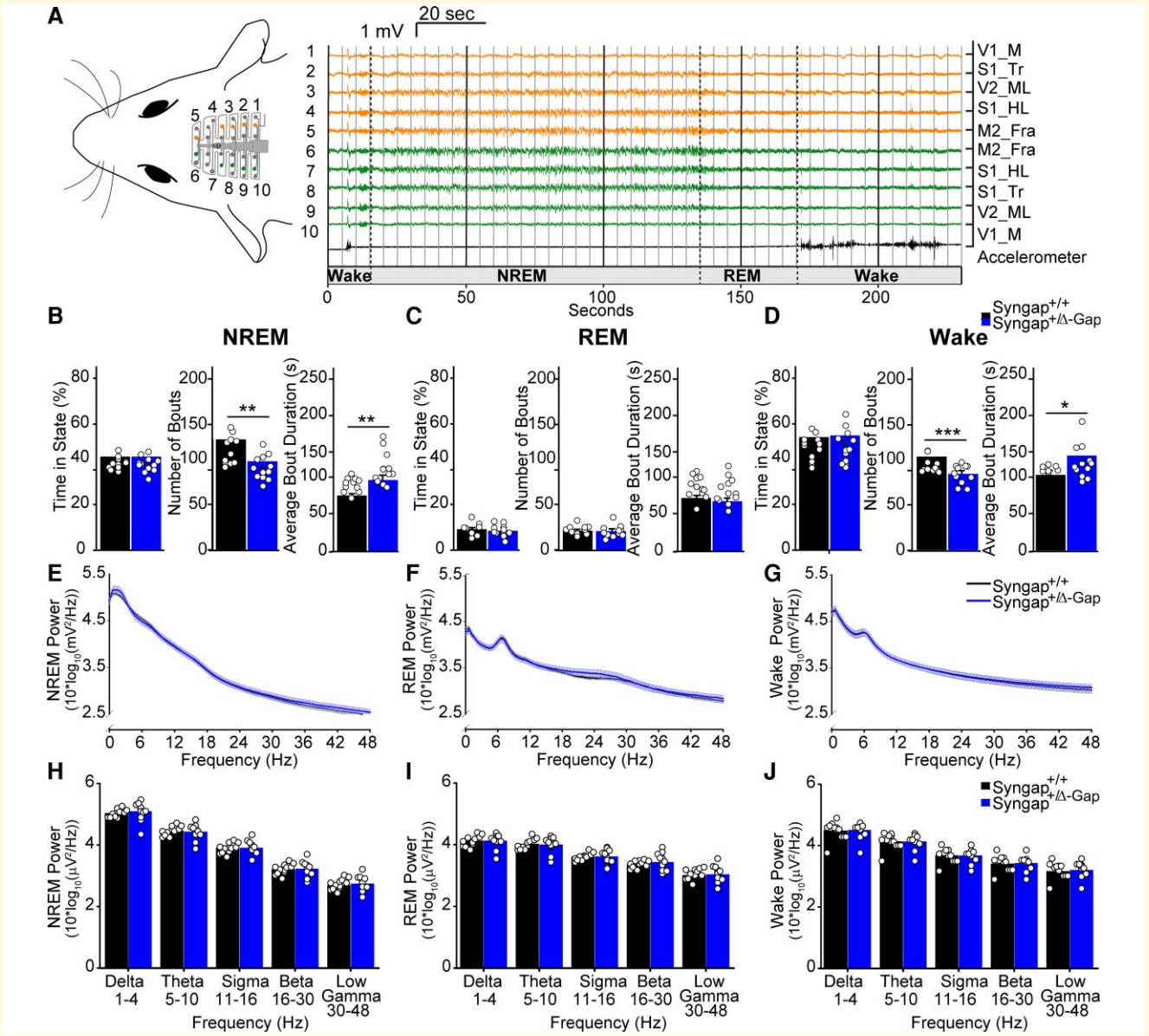

Figure 1 Brain state abnormalities in Syngap$^{+/\Delta-GAP}$ rats. (**A**) Schematic of a 32-channel skull-surface EEG implant illustrating approximate location of electrodes relative to the brain (left). Representative EEG voltage and accelerometer traces from numbered electrodes in schematic on left showing examples from NREM, REM and wake states (right). Dotted lines indicate brain state transitions, solid thin lines deliniate example 5 s brain state epochs. Electrode position abbreviations (Supplementary Figure 1) are displayed to the right of traces. Plots of percent time of 6 h recording, number of bouts and average bout duration for NREM (**B**), REM (**C**) and wake (**D**) brain states. Bars indicate mean values (mean ± SEM). Points correspond to values from individual rats. Number of bouts was significantly lower, while bout duration was significantly higher in Syngap$^{+/\Delta-GAP}$ rats (* = $P < 0.05$, ** = $P < 0.01$, *** P = <0.001, **** P = <0.0001, unpaired two-sample *t*-tests and two-sample Man–Whitney U rank sum tests specified in results text). Power spectrum estimates averaged across all NREM (**E**), REM (**F**) and wake (**G**) epochs. Error bars indicate SEM. Plots of average power in commonly used frequency bands during NREM (**H**), REM (**I**) and wake (**J**). Bars indicate mean values (mean ± SEM). Points correspond to values from individual rats. There were no significant differences across any bands between genotypes (two-way ANOVA specified in results text).

utilizing 6 h EEG (Fig. 1A, Supplementary Figure 1) recordings, when animals were in a quiet wake state.[17] To determine whether *Syngap*$^{+/\Delta-GAP}$ animals have abnormalities in their brain state distribution, we classified all individual 5 s recording epochs from those previous recordings as NREM sleep, REM sleep or wake (Fig. 1A). We found that *Syngap*$^{+/\Delta-GAP}$ rats spent an equivalent percentage of time in all states when compared with wild-type littermate controls (unpaired two-sample *t*-test for REM: DF = 22, T = 0.67, $P = 0.51$; NREM: DF = 22, T = 0.0025, $P = 0.1$; wake: DF = 22, T = 0.26, $P = 0.8$; Fig. 1B–D). Nonetheless, *Syngap*$^{+/\Delta-GAP}$ animals had a significantly lower number of

wake and NREM bouts, with REM bouts remaining unchanged (unpaired two-sample *t*-test for REM: DF = 22, T = 0.21, $P = 0.83$; wake: DF = 22, T = 3.8, $P = 0.00095$; NREM sleep: DF = 22, T = =3.5, $P = 0.002$; Fig. 1B–D). This coincided with increased average bout duration during wake and NREM and, no difference in REM bout duration (unpaired two-sample *t*-test for REM: DF = 22, T = 0.79, $P = 0.44$; wake: DF = 22, T = 2.57, $P = 0.017$; two-sample Mann–Whitney U rank sum test for NREM: U = 25, $P = 0.007$, Fig. 1B–D). Therefore, during 6 h recordings, *Syngap*$^{+/\Delta-GAP}$ rats display an abnormal brain state distribution.

We calculated the average EEG spectral power from one representative channel across all animals and epochs of each brain state and found no significant differences between *Syngap*$^{+/\Delta-GAP}$ rats and their wild-type littermates in commonly utilized frequency bands during NREM (two-way ANOVA, $P = 0.60$, F = 0.27, df = 1; Fig. 1E and H), REM (two-way ANOVA, $P = 0.68$, F = 0.17, df = 1; Fig. 1F and I) or wake (two-way ANOVA, $P = 0.60$, F = 0.27, df = 1; Fig. 1E and H), REM (two-way ANOVA, $P = 0.76$, F = 0.09, df = 1; Fig. 1G and J). These data show that *Syngap*$^{+/\Delta-GAP}$ rats display an abnormal sleep–wake distribution, although overall spectral properties across all frequency bands were unchanged.

Functional connectivity in syngap$^{+/\delta-GAP}$ rats

Abnormalities in synaptic connectivity may underlie the cognitive pathologies and epilepsy in *SYNGAP* haploinsufficiency.[28,29] Network activity pathophysiology in NDDs may be detected by analysing connectivity between EEG electrodes.[30] We therefore analysed the imaginary coherence, a generalization of correlation in the phase domain,[24] between voltage signals in our multi-site recordings during each brain state. Imaginary coherence decreases the likelihood of false dependencies between electrodes due to volume conductance by correlating between signal phases and not amplitude. We calculated the imaginary coherence for frequencies from 0 to 50 Hz for each brain state averaged across all epochs for all 496 combinations of electrode pairs from the 32 electrodes recorded. Since short- or long-distance connections may be differentially affected in NDDs and may display varying levels of correlation,[25] imaginary coherence values were then averaged by electrodes that were grouped by short or long distances (Fig. 2, Fig. 3, Supplementary Figure 1 and Supplementary Figure 3).

As rodent surface multi-site EEG probes have not been previously utilized to compare short- and long-distance electrode connectivity, we calculated whether there were differences between *Syngap*$^{+/\Delta-GAP}$ rats and wild-type controls using multiple distance thresholds separating groups of channels into short and long-distance channel combinations (Fig. 2, Fig. 3 and Supplementary Figure 3). The most striking differences occurred during NREM amongst short-distance pairs < 2 mm from each other (Fig. 2A–C and Supplementary Figure 3). When comparing commonly used frequency bands there was a clear, although none significant, trend towards decreased theta and sigma band imaginary coherence in *Syngap*$^{+/\Delta-GAP}$ rats (two-way ANOVA, $P = 0.06$, F = 3.54, df = 1, Fig. 2A and B). To identify abnormal frequency bands, we utilized an unbiased approach in which we compared the imaginary coherence between the two groups by statistically testing each individual 0.5 Hz frequency bin between 0.5 and 50 Hz and plotting *P*-values as a function of frequency.[26] We found clusters of consecutive significantly different frequencies with $P \leq 0.05$ corresponding to frequencies with significantly decreased *Syngap*$^{+/\Delta-GAP}$ imaginary coherence (two-sided randomization-based non-parametric test with cluster-based multiple comparison correction, Fig. 2C). These clusters occurred between 5 and 9 Hz and between 11.5 and 29.5 Hz. Furthermore, there was a striking subset of consecutive frequencies with lower *P*-values ($P \leq 0.01$) between 12 and 22 Hz (Fig. 2C and Supplementary Figure 3B). That range overlaps with the reported frequency range of sleep spindles (12–17 Hz), which are characteristic of NREM sleep and are thought to be critical for normal brain function and memory consolidation.[31,32] This cluster of significantly lower imaginary coherence frequencies suggests that connectivity may be compromised specifically during sleep spindles in *Syngap*$^{+/\Delta-GAP}$ animals in short-range distance electrode pairs.

There were no significant differences in commonly utilized frequency bands in short-distance electrodes < 2 mm during REM (two-way ANOVA, $P = 0.75$, F = 0.10, df = 1, Fig. 2D and E) although a trend towards significance in the sigma band was evident in wake periods (two-way ANOVA, $P = 0.10$, F = 2.72, df = 1, Fig. 2G and H). In contrast to NREM, there was only a small cluster of frequencies between 16 and 18 Hz during REM with $P \leq 0.05$ (two-sided randomization-based non-parametric test with cluster-based multiple comparison correction, Fig. 2F). While in wake there were no significantly different frequencies (two-sided randomization-based non-parametric test with cluster-based multiple comparison correction, Fig. 2I).

We also compared electrode pairs > 2 mm from each other as long-distance connectivity has been shown to be increased in children with other NDDs.[25] There were no significant differences in standard frequency bands between genotypes during NREM (two-way ANOVA, $P = 0.57$, F = 0.33, df = 1, Fig. 3A and B) or REM (two-way ANOVA, $P = 0.76$, F = 0.09, df = 1, Fig. 3E and F). This was confirmed by a lack of significantly different frequency clusters in both NREM and REM (two-sided randomization-based non-parametric test with cluster-based multiple comparison correction, Fig. 3C and F). However, a distinct none significant trend towards increased theta and sigma coherence in *Syngap*$^{+/\Delta-GAP}$ rats during wake in long-distance electrode pairs was detected (two-way ANOVA, $P = 0.06$, F = 3.72, df = 1, Fig. 3G and H). Clusters of consecutive significant frequencies, with $P \leq 0.05$ showing higher connectivity in *Syngap*$^{+/\Delta-GAP}$ rats, were present during wake in the theta range between 8 and 9.5 Hz, and in the sigma range between 14 and 16.5 Hz (two-sided randomization-based non-parametric test with cluster-based multiple comparison correction, Fig. 3I), suggesting hyper-connectivity phenotypes may be present during wake in *Syngap*$^{+/\Delta-GAP}$ rats.

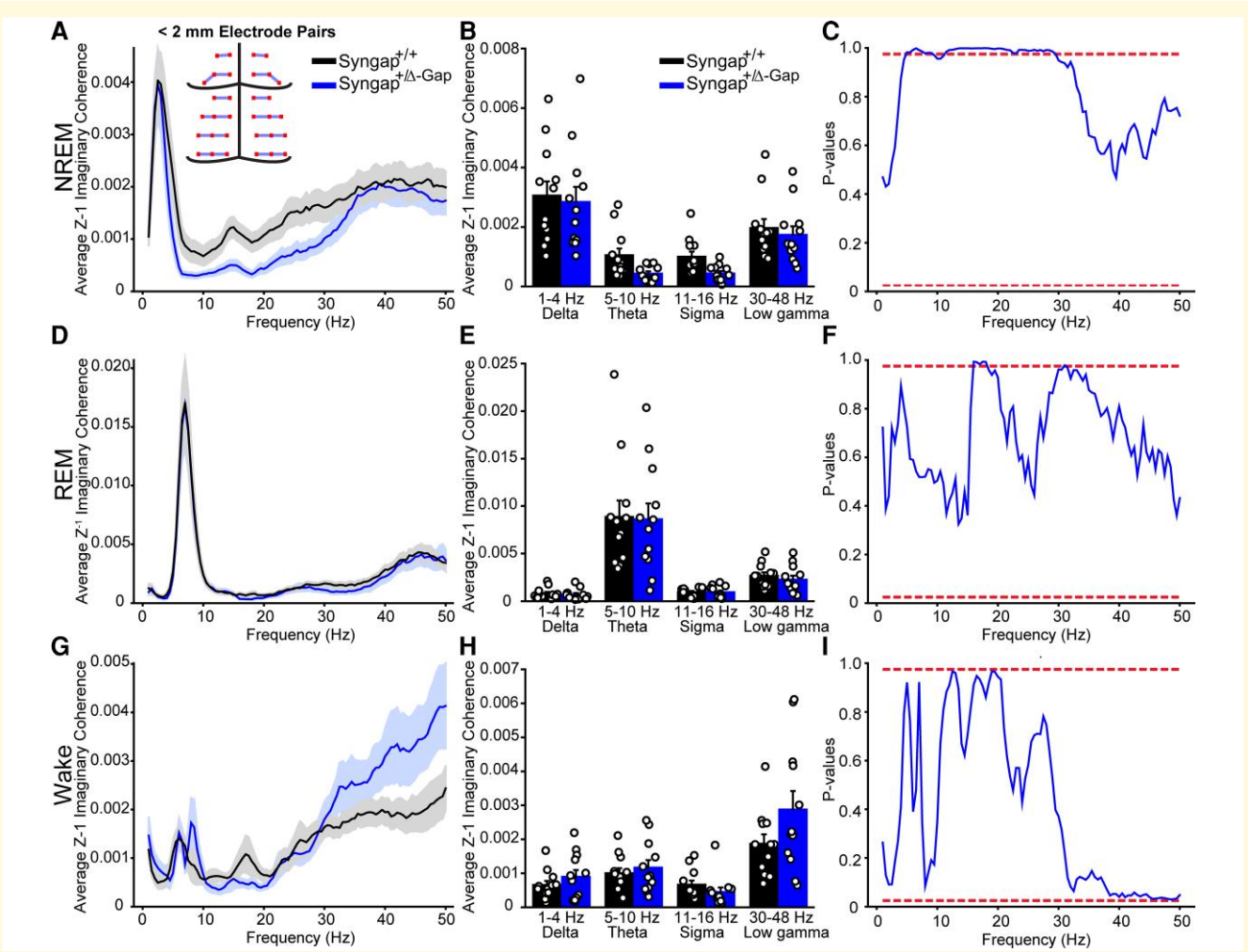

Figure 2 Decreased imaginary coherence during NREM in short-distance (< 2 mm apart) electrode pairs in Syngap$^{+/\Delta-GAP}$ rats. Average Z' imaginary coherence during NREM (**A**), REM (**D**) and wake (**G**) epochs. Shaded area indicates SEM. Inset in A: schematic of electrode pairs < 2 mm apart. Plots of average Z' imaginary coherence in commonly used frequency bands during NREM (**B**), REM (**E**) and wake (**H**). Lines indicate mean values (mean ± SEM). Points correspond to values from individual rats. There were no significant differences across any commonly used bands between genotypes (two-way ANOVA, $P = > 0.05$). Plots of *P*-values for cluster-based non-parametric tests during NREM (**C**), REM (**F**) and wake (**I**). Dotted red lines indicate two-sided *P*-value thresholds of ≥ 0.975 and ≤ 0.025 corresponding to significantly different thresholds equivalent to $P \leq 0.05$, two-sided. Note: A long cluster of significant frequencies was found during NREM between 11.5 and 29.5 Hz indicating a decrease in Z' imaginary coherence in Syngap$^{+/\Delta-GAP}$ rats.

Since short-distance electrode pairs had abnormalities in functional connectivity in *Syngap*$^{+/\Delta-GAP}$, we posited that cortical regions may have compromised imaginary coherence between each other. We tested whether specific cortical areas had disruptions in functional connectivity by averaging voltage signals from channels in three rostral to caudal bilateral regions (Supplementary Figure 4A) and by calculating the imaginary coherence between regions during NREM, as our primary abnormality was in the 11.5–29.5 frequency range in that brain state. However, we found no clusters of significant values in any comparison between regions (Supplementary Figure 4B), suggesting that the abnormality in NREM is specific to short-distance channels.

Overall, these data show that *Syngap*$^{+/\Delta-GAP}$ rats have connectivity abnormalities between electrode pairs located at varying distances from each other, with particularly striking deficiencies in imaginary coherence during NREM amongst short-distance pairs of electrodes. Electrodes < 2 mm from each other mainly correspond to pairs of electrodes overlaying cortical areas with equivalent functionality, such as visual, motor or somatosensory areas (Fig. 2A and Supplementary Figure 1), suggesting that imaginary coherence abnormalities occur in local connections within cortical regions with a defined function.

SWDs and brain state abnormalities in *syngap*$^{+/\delta-GAP}$ rats

A critical question in epileptic encephalopathies such as SYNGAP1 haploinsufficiency is whether the presence of

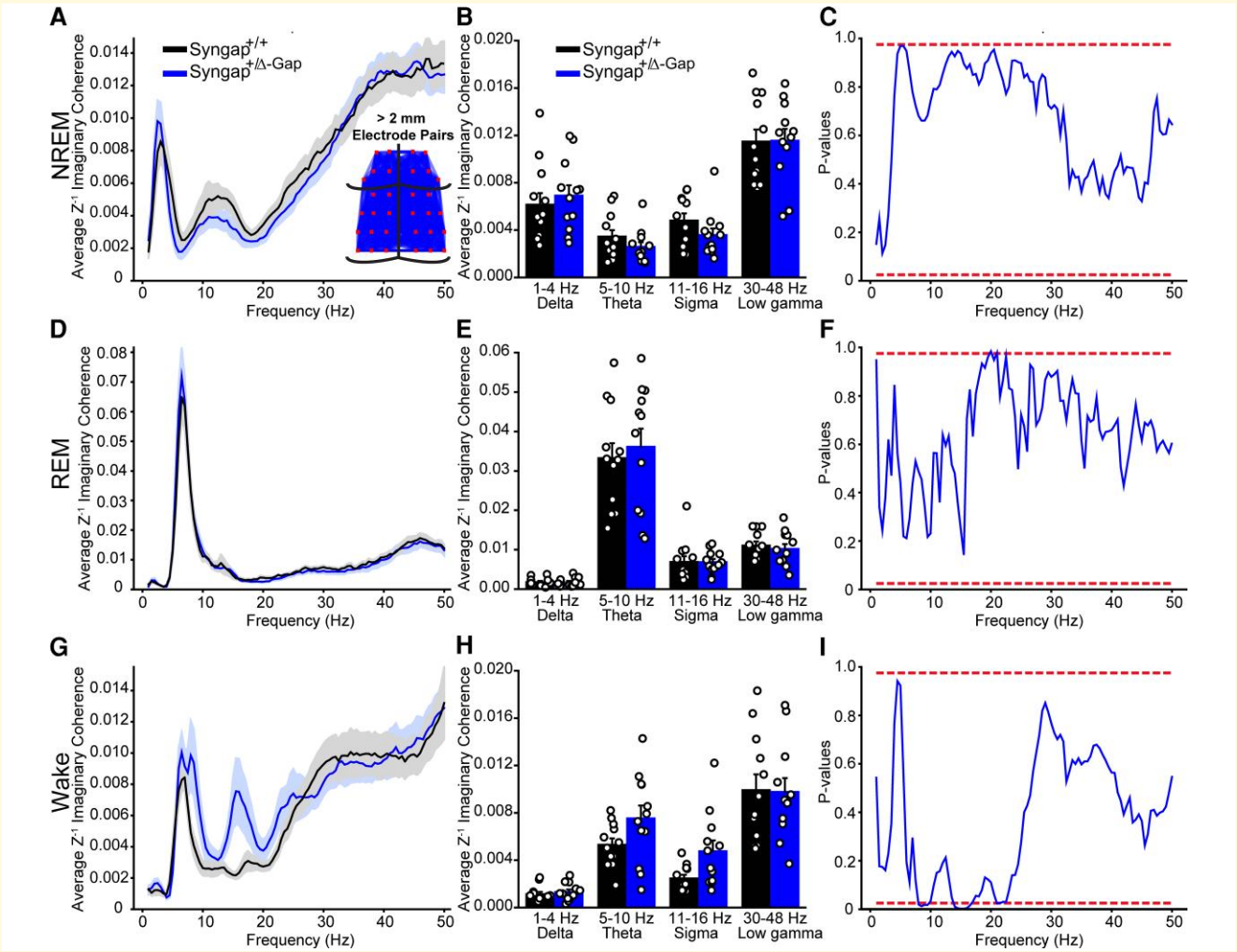

Figure 3 Increased imaginary coherence during wake in long-distance (> 2 mm apart) electrode pairs in Syngap$^{+/\Delta-GAP}$ rats. Average Z' imaginary coherence during REM (**A**), NREM (**D**) and wake (**G**) epochs. Shaded area indicates SEM. Inset in A: schematic of electrode pairs > 2 mm apart. Plots of average Z' imaginary coherence in commonly used frequency bands during NREM (**B**), REM (**E**) and wake (**H**). Bars indicate mean values (mean ± SEM). Points correspond to values from individual rats. There were no significant differences across any commonly used bands between genotypes (two-way ANOVA, $P = > 0.05$). Plots of *P*-values for cluster-based non-parametric test during NREM (**C**), REM (**F**) and wake (**I**). Dotted red lines indicate two-sided *P*-value thresholds of ≥ 0.975 and ≤ 0.025 corresponding to significantly different thresholds equivalent to $P \leq 0.05$, two-sided. Note: Clusters of significant frequencies were found during wake between 8 and 9.5 Hz and 14 and 16.5 Hz indicating an increase in Z' imaginary coherence in Syngap$^{+/\Delta-GAP}$ rats.

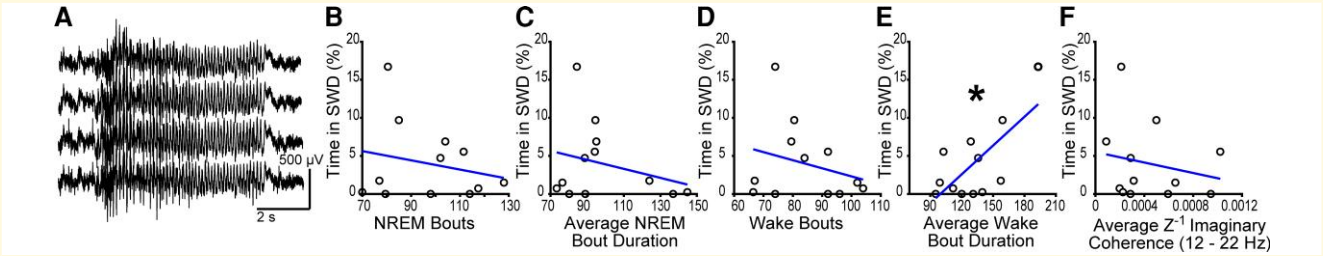

Figure 4 SWDs are uncorrelated to sleep and connectivity abnormalities in Syngap$^{+/\Delta-GAP}$ animals. (**A**) Representative EEG traces during a SWD in five electrodes in a Syngap$^{+/\Delta-GAP}$ rat. Plots of NREM bouts (**B**), average NREM bout duration (**C**), wake bouts (**D**), average wake bout duration (**E**), and average Z^{-1} imaginary coherence in the 12–22 Hz band (**F**) plotted against percentage recorded time of SWD occurrence. Points correspond to values from individual rats with a line representing best fit. There was a significant correlation between average wake bout duration and percent time in SWDs in Syngap$^{+/\Delta-GAP}$ rats with no differences in the other metrics (* = $P < 0.05$, Pearson correlation).

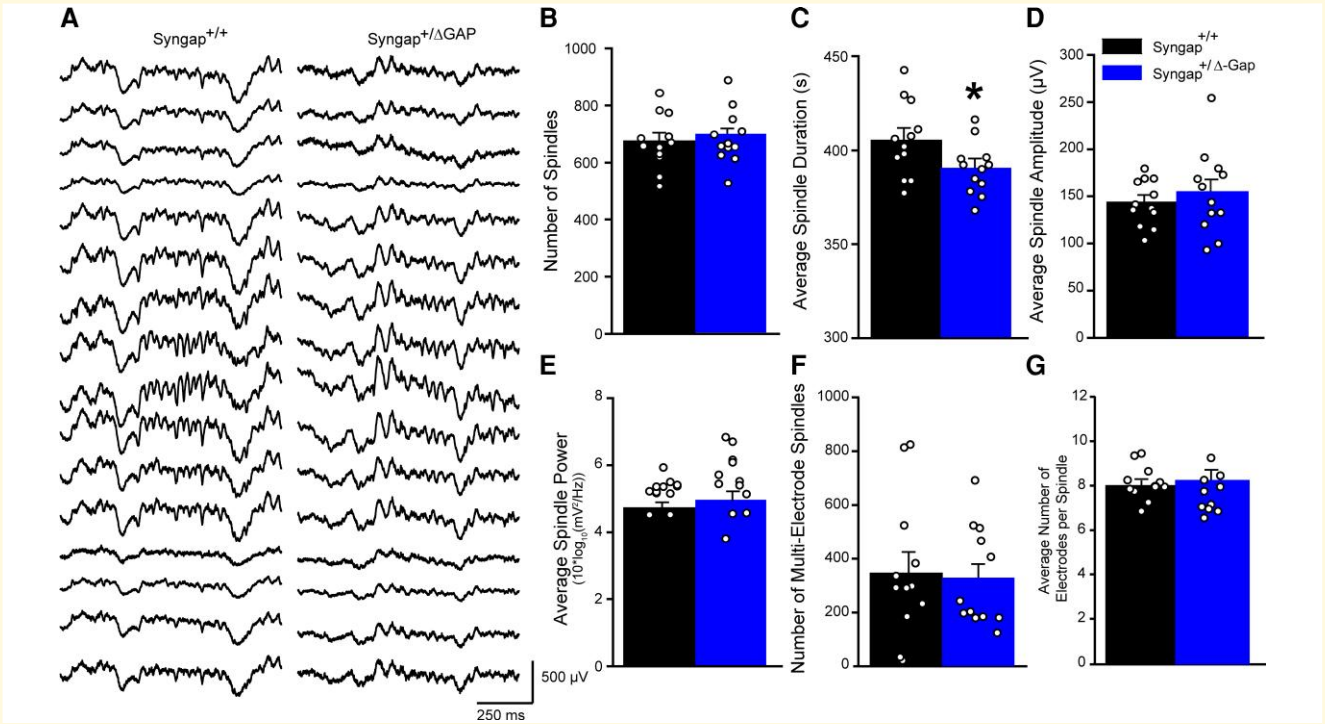

Figure 5 Sleep spindles are unaltered in Syngap$^{+/\Delta-GAP}$ animals. (**A**) Representative EEG traces during sleep spindles in 16 electrodes in Syngap$^{+/+}$ (left) and Syngap$^{+/\Delta-GAP}$ (right) rats. Plots of spindle number (**B**), average duration (**C**), average amplitude (**D**), average power in the spindle frequency band (12–17 Hz) (**E**), multi-electrode spindles (**F**) and average electrodes per spindle (**G**). Bars indicate mean values (mean ± SEM). Points correspond to values from individual rats. There was a significant decrease in spindle duration in Syngap$^{+/\Delta-GAP}$ rats with no differences in the other metrics (* = $P < 0.05$, unpaired two-sample *t*-tests).

seizures influences other neurodevelopmental phenotypes. We previously reported that SWDs (Fig. 4A), the electrophysiological correlate of absence seizures, are significantly more prevalent in Syngap$^{+/\Delta-GAP}$ rats than in littermate controls.[17] We hypothesized that SWDs may correlate with time spent in specific brain states as well as cortical connectivity. We tested whether the percentage amount of time spent in SWDs was correlated to sleep abnormalities (Fig. 1C, D) and the average imaginary coherence values during NREM in the frequency range between 12 and 22 Hz where there were connectivity deficits with low *P*-values ($P \leq 0.01$) (Fig. 2A and C). SWDs in Syngap$^{+/\Delta-GAP}$ rats were not significantly correlated to number of NREM bouts (Pearson correlation, DF = 1, F = 0.511, R = −0.22, $P = 0.491$, Fig. 4B), average NREM bout duration (Pearson correlation, DF = 1, F = 0.803, R = −0.273, $P = 0.391$, Fig. 4C), or number of wake bouts (Pearson correlation, DF = 1, F = 0.766, R = −0.267, $P = 0.402$, Fig. 4D). SWDs were significantly correlated to average wake bout duration (Pearson correlation, DF = 1, F = 9.833, R = 0.704, $P = 0.0106$, Fig. 4E). However, we found no significant correlation between SWD time and the primary average imaginary coherence difference recorded in the 12–22 Hz frequency range during NREM (Pearson correlation, DF = 1, F = 0.429, R = −0.203, $P = 0.527$, Fig. 4F). Only average wake bout duration correlates with SWDs, suggesting that absence seizures only minimally affect sleep and connectivity abnormalities.

Sleep spindles in *Syngap*$^{+/\delta-GAP}$ rats

Due to the reduction in average imaginary coherence in the sleep spindle frequency range in short-distance electrode combinations, we assessed whether sleep spindles were abnormal in *Syngap*$^{+/\Delta-GAP}$ rats (Fig. 5A). We first automatically detected spindles across animals from a single channel, over the right primary somatosensory cortex (Supplementary Figure 1), to determine whether spindle number and duration is altered in *Syngap*$^{+/\Delta-GAP}$ rats. There was no significant difference in the total number of spindles detected (two-sample unpaired *t*-test, DF = 22, T = 0.59, $P = 0.56$, Fig. 5B) although there was a small decrease in the average duration of spindles in *Syngap*$^{+/\Delta-GAP}$ rats when compared with wild-type littermates (two-sample unpaired *t*-test, DF = 22, T = 2.19, $P = 0.039$, Fig. 5C). The average spindle amplitude was not significantly different between both genotypes (two-sample unpaired *t*-test, DF = 22, T = 0.75, $P = 0.461$, Fig. 5D) nor was the average power after spindle detection in the 12–17 Hz band (Mann–Whitney U test, U = 52, $P = 0.26$, Fig. 5E). We then automatically detected spindles across all channels during NREM to assess whether there was a deficit between how spindles spread between short-distance pairs of electrodes. We found that there was no significant difference between *Syngap*$^{+/\Delta-GAP}$ rats and wild-type littermates in both the number of times that a

spindle was simultaneously identified in more than one electrode (two-sample unpaired *t*-test, DF = 22, T = 1.78, *P* = 0.26 Fig. 5F) and the number of electrodes in which a spindle was present, when it was detected in more than one electrode (two-sample unpaired *t*-test, DF = 22, T = −0.92, *P* = 0.37, Fig. 5G). These results show that spindle occurrence, amplitude, spectral power and detection of spindles throughout the cortex are unchanged in *Syngap*$^{+/\Delta-GAP}$ rats.

Dynamic functional connectivity in *Syngap*$^{+/\delta-GAP}$ rats during sleep spindles

We hypothesized that the significant reduction in average imaginary coherence in *Syngap*$^{+/\Delta-GAP}$ rats during NREM in short-distance electrode pairs may be a consequence of deficits in connectivity across channels during spindles. We therefore calculated average imaginary coherograms during spindles across all electrode combinations at distances ≤ 2 mm from each other for each animal, and we identified the total number of time–frequency bins in the coherograms that exceeded 70% of the maximum connectivity detected in each individual animal (Fig. 5A). We found that *Syngap*$^{+/\Delta-GAP}$ rats had significantly decreased total high-connectivity time–frequency bins from average coherograms when compared with wild-type controls (two-sample unpaired *t*-test, DF = 22, T = −2.39, *P* = 0.03, Fig. 6B). This coincided with a significant increase in the spectral frequency at which high-connectivity time–frequency bins occurred (two-sample unpaired *t*-test, DF = 22, T = 2.13, *P* = 0.04, Fig. 6C).

These data show that there is a deficit in the occurrences of high functional connectivity in *Syngap*$^{+/\Delta-GAP}$ rats during spindles that may contribute to the overall decrease in imaginary coherence during NREM amongst short-distance electrode pairs.

We also compared the average values of imaginary coherence from coherograms during the entire length of spindles between the two genotypes and found that there was no significant reduction both across averages from all 496 channel combinations (two-sample unpaired *t*-test, DF = 22, T = 1.34, *P* = 0.19, Fig. 7B) and across averages from pairs of channels ≤ 2 mm from each other (two-sample unpaired *t*-test, DF = 22, T = 1.72, *P* = 0.10, Fig. 7B). This suggests that what contributes to decreased spindle coherence in short-distance channels is the reduction of occurrences of high-connectivity during spindles and not the overall average across the entire 12–17 Hz range and time preceding and following the start of spindles.

It is possible that specific channel combinations that are not organized by distance, but by cortical location may have altered coherence during spindles. We therefore analysed whether specific channel pairs had significantly decreased connectivity when compared across animals and we found 45 combinations of channels where the imaginary coherence was significantly decreased in *Syngap*$^{+/\Delta-GAP}$ rats between 12 and 17 Hz (Fig. 6A and Supplementary Table 1). These channels were located caudal to bregma predominantly on the right posterior hemisphere over somatosensory, association and visual cortices (Fig. 6A and Supplementary Figure 1). Some long-range and interhemispheric channel pairs also showed differences between the groups (Fig. 7A). When we evaluated the average imaginary coherence for these

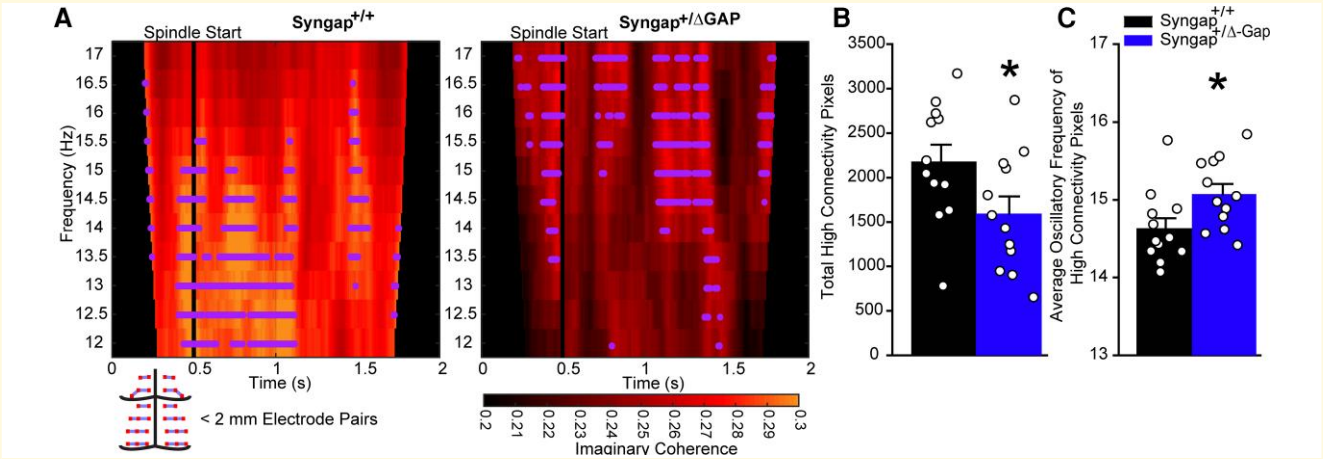

Figure 6 The occurrences of high-connectivity during sleep spindles was reduced in short-distance (< 2 mm apart) electrode pairs in Syngap$^{+/\Delta-GAP}$ rats. (**A**) Average coherograms across electrode pairs preceding and during sleep spindles (top). Dots indicate instances of high-connectivity (70% of maximum average connectivity time–frequency bin detected in each animal). Schematic of electrode pairs < 2 mm apart and imaginary coherence colour scale (below). Plots of total high-connectivity time–frequency bins (**B**) and average oscillatory frequency of high-connectivity pixels per spindle (**C**). Bars indicate mean values (mean ± SEM). Points correspond to values from individual rats. There was a significant decrease in high-connectivity (two-sample unpaired *t*-test, DF = 22, T = −2.39, *P* = 0.03) time–frequency bins and, a significant increase in the average oscillatory frequency of high-connectivity time–frequency bins (two-sample unpaired *t*-test, DF = 22, T = 2.13, *P* = 0.04) in Syngap$^{+/\Delta-GAP}$ animals.

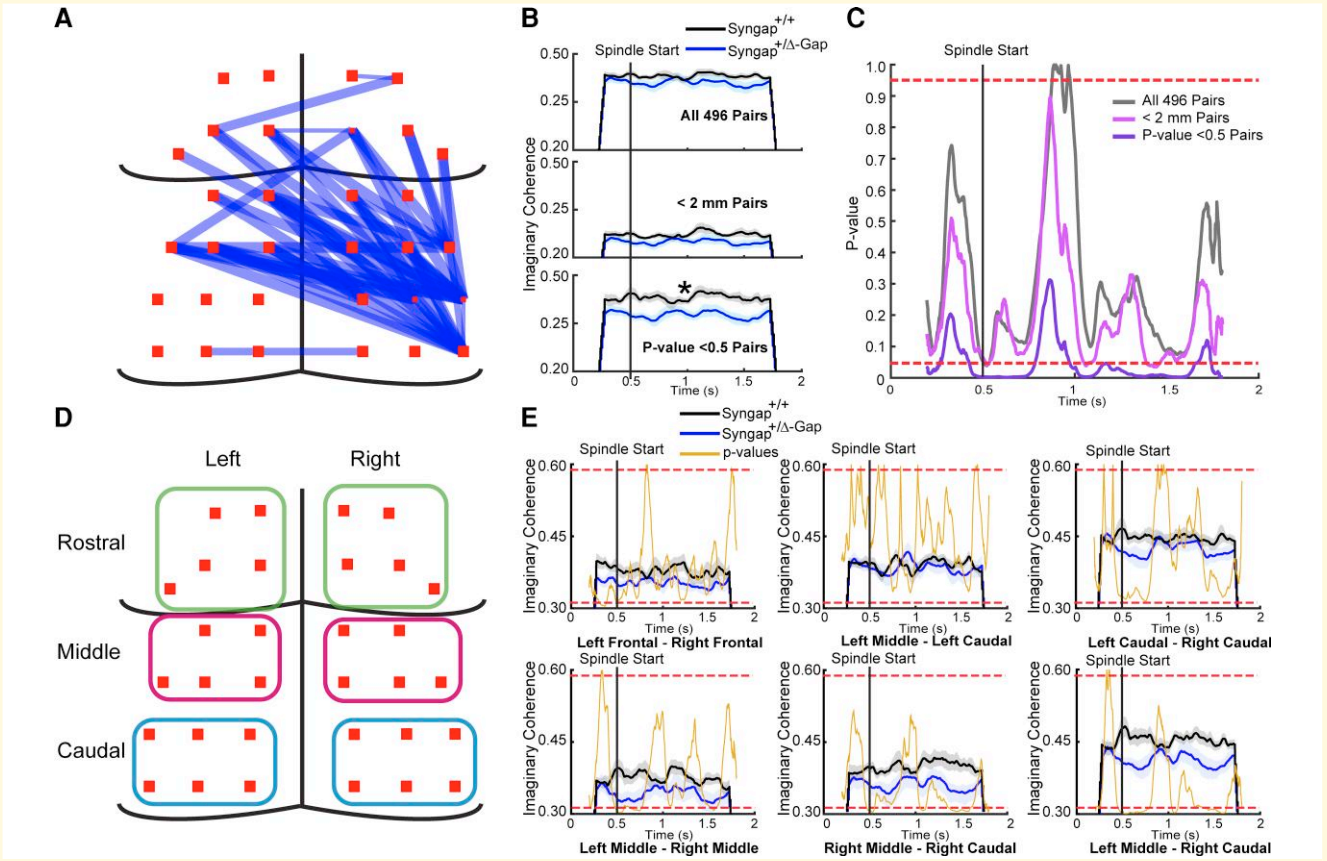

Figure 7 A specific subset of electrode pairs displays significantly reduced imaginary coherence during sleep spindles in Syngap$^{+/\Delta-GAP}$ rats. (**A**) Schematic of electrodes pairs with a significant reduction in imaginary coherence during sleep spindles in Syngap$^{+/\Delta-GAP}$ animals. Note: Thickness of lines indicate relative significance level detailed in Supplementary Table 1. (**B**) Average imaginary coherence preceding and during sleep spindles for all 496 (top), <2 mm apart (middle) and individually significant (bottom) electrode pairs (Supplementary Table 1). Shaded area indicates SEM. (**C**) Plots of *P*-values for cluster-based non-parametric test preceding and during sleep spindles for all 496, <2 mm apart and individually significant electrode pairs. Dotted horizaontal lines indicate two-sided *P*-value thresholds of ≥ 0.975 and ≤ 0.025 corresponding to significantly different thresholds equivalent to $P \leq 0.05$. Note: Clusters of significant times during sleep spindles were primarily found in individually significant electrode pairs in Syngap$^{+/\Delta-GAP}$ rats. (**D**) Schematic of regional areas averaged and in which dynamic imaginary coherence was calculated. (**E**) Plots of average imaginary coherence preceding and during sleep spindles with *P*-values for cluster-based non-parametric test. Dotted red lines indicate two-sided *P*-value thresholds of ≥ 0.975 and ≤ 0.025 corresponding to significantly different thresholds equivalent to $P \leq 0.05$, two-sided. Note: Clusters of significant times were only found in left middle—right middle, right middle—right caudal and left middle—right caudal comparisons. Other none significant comparisons are displayed in Supplementary Figure 4.

channel combinations, we found a significant decrease in *Syngap*$^{+/\Delta-GAP}$ rats compared to controls (two-sample unpaired *t*-test, DF = 22, T = 3.04, $P = 0.006$, Fig. 7B). This was confirmed by comparing specific time points before and during spindles between the two genotypes utilizing the different combinations of electrode pairs. Clear and long clusters of consecutively significant timepoints, $P \leq 0.05$, were present when utilizing the 45 channels with significantly decreased coherence and not when utilizing all 496 pairs or electrodes <2 mm from each other (two-sided randomization-based non-parametric test with cluster-based multiple comparison correction, Fig. 7C).

We then tested whether specific cortical areas had significant differences in dynamic connectivity during spindles. Voltages during all spindles were averaged across channels in specific regions (Fig. 7D) and dynamic imaginary coherence was calculated between regional pairs (Fig. 7E, Supplementary Figure 4). Long clusters of significantly different time points during spindles were only found in regional pairs in the right middle—left middle, right middle—right caudal and left middle—right caudal—regional pairs (Fig. 7E), which are regions that overlap with the 45 channel pairs identified that had significantly decreased connectivity (Fig. 7A). The three regional pairs had long clusters of timepoints in which the imaginary coherence was significantly decreased *Syngap*$^{+/\Delta-GAP}$ rats at approximately 500 ms, which corresponds to the start of the spindle (two-sided randomization-based non-parametric test with cluster-based multiple comparison correction, right middle—left middle between 497 and 567 ms, right middle—right caudal

between 466 and 754 ms, left middle—right caudal 490 and 545 ms). In the right middle—right caudal and left middle—right caudal regional pairs, there were a second cluster of significant times after approximately 1000 ms (two-sided randomization-based non-parametric test with cluster-based multiple comparison correction, right middle—right caudal between 1045 and 1093 ms, left middle—right caudal 1077 and 1087 ms) and 1500 ms (two-sided randomization-based non-parametric test with cluster-based multiple comparison correction, right middle—right caudal between 1525 and 1627 ms, left middle—right caudal 1529 and 1584 ms). This indicates that the imaginary coherence between specific sets of regional and channel connections is significantly reduced during sleep spindles in *Syngap*$^{+/\Delta-GAP}$ rats compared with wild-type controls.

Overall, these results show that there are deficits in instances of high functional connectivity during spindles amongst electrode combinations at short distances from each other, while a subset of electrode combinations and regions have a higher degree of connectivity deficits, suggesting potential abnormalities in *Syngap*$^{+/\Delta-GAP}$ rats in specific underlying cortical anatomy.

Discussion

We show that brain states are altered in *Syngap*$^{+/\Delta-GAP}$ animals as the number of NREM and wake bouts are decreased. Nonetheless a corresponding increase in average NREM and wake bout duration in *Syngap*$^{+/\Delta-GAP}$ rats resulted in an equal percentage of time spent in NREM, REM and wake states when compared with wild-type controls. Although no significant differences in spectral power or imaginary coherence were detected in commonly utilized frequency bands; when imagery coherence was compared between genotypes with a non-biased non-parametric method, clear decreases in *Syngap*$^{+/\Delta-GAP}$ animals in electrode pairs < 2 mm apart during NREM between 11.5 and 29.5 Hz were present. The overlap of the decrease in imaginary coherence during NREM with the sleep spindle frequency range amongst pairs of electrodes < 2 mm apart, prompted an in-depth analysis in sleep spindle properties. The occurrence, amplitude, power and detection of sleep spindles across multiple electrodes was unchanged in *Syngap*$^{+/\Delta-GAP}$ rats with only a small decrease in duration detected. Notwithstanding, dynamic coherence analysis revealed that during spindles, instances of high-connectivity were decreased in *Syngap*$^{+/\Delta-GAP}$ animals, which was accompanied by an increase in average high-connectivity imaginary coherence frequency. Finally, the average coherence during spindles amongst all pairs of electrodes, as well as those < 2 mm apart, was not significantly different between genotypes despite the decrease in the instances of high-connectivity for electrodes < 2 mm in *Syngap*$^{+/\Delta-GAP}$ rats. However, by identifying a subset of electrodes with significantly decreased connectivity during spindles in *Syngap*$^{+/\Delta-GAP}$ animals, we found that as a group, these electrodes did show average decreased connectivity. These electrodes were primarily located in the right caudal hemisphere, suggesting that cortical dynamics at this location may be particularly affected by the *SYNGAP1* mutation.

Absence seizures are the most prevalent seizure type in *SYNGAP1* haploinsufficiency patients, with 53/57 cases having absence seizures in a recent clinical report.[3] *Syngap*$^{+/\Delta-GAP}$ are to our knowledge, the only pre-clinical model of *SYNGAP1* with spontaneous absence seizures.[17] Replication of such an important phenotype suggests that this model has a high face validity and therefore biomarkers identified here may have particular translational relevance.

The percent recording time spent in SWDs was positively correlated with wake bout duration, but it was not correlated with the number of NREM bouts or their duration, the number of wake bouts or imaginary coherence values between electrodes < 2 mm apart during spindles in *Syngap*$^{+/\Delta-GAP}$. These data suggest that deletion of the C2 and GAP domains of *SYNGAP1* may result in independent circuit mechanisms leading to sleep and connectivity deficits and seizures.

Difficulties in both initiating and maintaining sleep as well as reduced overall sleep duration have been reported in individuals with *SYNGAP1* mutations.[3,8,9] In our previous work we performed 6 hr recordings EEG recordings and found that *Syngap*$^{+/\Delta-GAP}$ animals displayed absence seizures at a higher rate than controls.[17] We have further analysed these recordings, which were made during daylight hours, resulting in rats spending approximately half of the recording time asleep. Despite recent clinical reports, we found that the overall time spent asleep was not different from littermate controls in mutant animals. Nonetheless, the number of times that *Syngap*$^{+/\Delta-GAP}$ rats entered NREM or wake brain states was decreased. Interestingly, there was also an increase in the duration of NREM and wake bouts, which suggest that overall sleep structure is compromised in these animals. Since sleep is intermingled with wake states throughout the day in rats, full-day circadian recordings may identify further sleep abnormalities in this mutant line.

EEG has been suggested as a potential method to identify clinical biomarkers in NDDs [33] and indeed analysis of EEG connectivity and networks have yielded specific signatures for epilepsy and autism.[25,34] For example, in temporal lobe epilepsy, high-frequency oscillations recorded with intracranial EEG can be utilized to identify the seizure onset zone and improve the efficacy of surgical brain resection to control seizures.[35] Furthermore, it has been proposed that analysing the spatiotemporal coherence of high-frequency oscillations can yield more spatially refined targeting of the seizure onset zone.[36] Modifying network oscillatory rhythms has proven effective in curtailing seizures in rodent models of temporal lobe epilepsy[37] and may be an important mechanistic component of how deep brain stimulation of the anterior nucleus of the thalamus controls seizures in patients.[38] In tuberous sclerosis complex EEG coherence abnormalities in infants are associated with the development of autism spectrum disorders,[39] while a high level of EEG mutual information, another metric of connectivity, predicts the emergence of epileptic spasms.[40] In patients with Lennox Gastaut syndrome and Dravet

syndrome, severe epileptic encephalopathies with refractory seizures, abnormalities in phase coherence and graph theory metrics predict the effectiveness of cannabidiol treatment.[41]

Similarly to human EEG, it may be that abnormalities present in brain circuit activity are only detectable through intracranial recordings, such as with high-frequency oscillations in temporal lobe epilepsy, which are reduced in duration and amplitude in surface recordings,[42] with higher frequency oscillations being more vulnerable to skull and skin tissue interference,[43] which is why we focused our analysis on frequencies lower than 50 Hz.

Here, we performed analysis on the connectivity between electrode pairs from our multi-site EEG probes. We utilized imaginary coherence since the likelihood of volume conductance artefacts with a method analysing amplitude correlations, may be higher with the reduced skull size of rats compared with humans.

We separated electrode pairs between short- and long-distance groups and averaged the overall coherence within these groups. We performed comparisons with varying threshold distances separating short- and long-distance electrode pair groups and found that the clearest deficits in connectivity in *Syngap*$^{+/\Delta-GAP}$ rats occurred during NREM in short-distance electrodes < 2 mm. SYNGAP is primarily located in excitatory synapses and is a key regulator of spine formation[14–16]. Cortical pyramidal cells form most of their intracortical connections with neighbours in close proximity.[44] Electrodes with < 2 mm distance from each other are mainly located over cortical areas with similar function such as motor, visual or somatosensory processing (Fig. 2A and Supplementary Figure 1). These data suggest that in *SYNGAP1* haploinsufficiency human patients there may be a deficit in connections within regions of cortex with a common function, which may be heightened during cortical activity in NREM.

Across brain states, there were no significant differences in power, although there was a reduction in imaginary coherence between short-distance electrodes during NREM and an increase in imaginary coherence between long-distance electrodes during wake. Imaginary coherence has been proposed as a method to more accurately measure the interactions between brain regions.[24] Power at an individual channel can be independent of the coherence measured between that channel and another. In fact, in recent work in Angelman syndrome patients, abnormalities in power at specific bands are not necessarily reflected in coherence calculations, and vice versa, coherence abnormalities are often associated with no changes in power.[12,25]

One of the characteristics of NREM are sleep spindles, which are thought to be critical for memory processes,[32] and lower imaginary coherence in the spindle frequency range led us to investigate their characteristics in *Syngap*$^{+/\Delta-GAP}$ animals. We found that their overall characteristics were unaffected, as well as the average connectivity during a spindle. Nonetheless, brief periods of high-connectivity were significantly decreased in *Syngap*$^{+/\Delta-GAP}$ rats, with a concurrent increase in the oscillatory frequency at which these high-connectivity events occurred. How cortical neuronal populations interact during sleep spindles may be compromised in *Syngap*$^{+/\Delta-GAP}$ animals. Analysis of sleep spindle connectivity between individual channel combinations showed that a subgroup of connections had significantly lower imaginary coherence in *Syngap*$^{+/\Delta-GAP}$ rats. This area is located over the right somatosensory, association and visual cortices, which may be more vulnerable to deficits due to *SYNGAP1* mutation. Some interhemispheric connectivity abnormalities may also be present, although the overall average imaginary coherence between long-distance connections was not significantly altered during NREM (Fig. 3C). Nonetheless, when we compared dynamic imaginary coherence by specific cortical regions (Fig. 7D, E), we found that these overlapped with significantly different channel combinations. The locations with significant decreases in connectivity were located between the left middle cortical area and the contralateral middle and caudal regions. There was also a deficit between the middle and caudal areas over the right hemisphere. These data suggest that these regions may be specifically affected in *Syngap*$^{+/\Delta-GAP}$ rats.

Finally, we saw that despite decreases in the overall number of NREM and wake bouts, the overall time spent in those states was not decreased due to their increased duration in *Syngap*$^{+/\Delta-GAP}$ animals. Interestingly, we also saw decreased connectivity during NREM in the sigma range in mutant animals, which was accompanied by increased connectivity in the theta and sigma range during wake. A degree of homeostatic adaptation may be occurring in mutant animals to counteract the effects of the mutation during different brain states.

In conclusion, we report sleep abnormalities and differences in connectivity during specific brain states in the *Syngap*$^{+/\Delta-GAP}$ rat model. Imaginary coherence analysis of EEG data may have value as a clinical biomarker and this analysis points to specific neuronal populations that may be affected by the mutation.

Acknowledgements

For the purpose of open access, the author has applied a CC BY public copyright licence to any Author Accepted Manuscript version arising from this submission.

Funding

The work performed here was funded by The Simons Initiative for the Developing Brain, the Patrick Wild Centre, an Epilepsy Research United Kingdom grant [F1603] and a Wellcome Trust Institutional Support Fund grant [204804/Z/16/Z].

Competing interests

The authors report no competing interests.

Supplementary material

Supplementary material is available at *Brain Communications* online.

References

1. Parikshak NN, Luo R, Zhang A, *et al.* Integrative functional genomic analyses implicate specific molecular pathways and circuits in autism. *Cell*. 2013;155(5):1008-1021.
2. Hamdan FF, Gauthier J, Spiegelman D, *et al.* Mutations in SYNGAP1 in autosomal nonsyndromic mental retardation F. *N Engl J Med*. 2009;360(6):599-605.
3. Vlaskamp DRM, Shaw BJ, Burgess R, *et al.* SYNGAP1 Encephalopathy: A distinctive generalized developmental and epileptic encephalopathy. *Neurology*. 2019;92(2):E96-E107.
4. Deciphering Developmental Disorders. Europe PMC funders group large-scale discovery of novel genetic causes of developmental disorders. *Nature*. 2015;519(7542):223-228.
5. Deciphering Developmental Disorders. Prevalence and architecture of de novo mutations in developmental disorders. *Nature*. 2017; 542(7642):433-438.
6. Satterstrom FK, Kosmicki JA, Wang J, *et al.* Large-Scale exome sequencing study implicates both developmental and functional changes in the neurobiology of autism. *Cell*. 2020;180(3):568-584.e23.
7. Carvill GL, Heavin SB, Yendle SC, *et al.* Targeted resequencing in epileptic encephalopathies identifies de novo mutations in CHD2 and SYNGAP1. *Nat Publ Gr*. 2013;45(7):825-830.
8. Jimenez-Gomez A, Niu S, Andujar-Perez F, *et al.* Phenotypic characterization of individuals with SYNGAP1 pathogenic variants reveals a potential correlation between posterior dominant rhythm and developmental progression. *J Neurodev Disord*. 2019;11(1):1-11.
9. Smith-Hicks C, Wright D, Kenny A, *et al.* Sleep abnormalities in the synaptopathies—Syngap1-related intellectual disability and phelan–mcdermid syndrome. *Brain Sci*. 2021;11(9):1229–12210.
10. Sahin M, Jones SR, Sweeney JA, *et al.* Discovering translational biomarkers in neurodevelopmental disorders. *Nat Rev Drug Discov*. 2018;18(april):235-236.
11. Lau-zhu A, Lau MPH, Mcloughlin G. Mobile EEG in research on neurodevelopmental disorders: Opportunities and challenges. *Dev Cogn Neurosci*. 2019;36(March):100635.
12. Sidorov MS, Deck GM, Dolatshahi M, *et al.* Delta rhythmicity is a reliable EEG biomarker in angelman syndrome: A parallel mouse and human analysis. *J Neurodev Disord*. 2017;9(1):1-14.
13. Lopez-Rivera JA, Perez-Palma E, Symonds J, *et al.* A catalogue of new incidence estimates of monogenic neurodevelopmental disorders caused by de novo variants. *Brain*. 2020;143:1099-1105.
14. Chen HJ, Rojas-Soto M, Oguni A, Kennedy MB. A synaptic ras-GTPase activating protein (p135 SynGAP) inhibited by CaM kinase II. *Neuron*. 1998;20(5):895-904.
15. Kim JH, Liao D, Lau LF, Huganir RL. SynGAP: A synaptic RasGAP that associates with the PSD-95/SAP90 protein family. *Neuron*. 1998;20(4):683-691.
16. Gamache TR, Araki Y, Huganir RL. Twenty years of syngap research: From synapses to cognition. *J Neurosci*. 2020;40(8):1596-1605.
17. Katsanevaki D, Till MS, Buller-Peralta I, *et al.* Heterozygous deletion of SYNGAP enzymatic domains in rats causes selective learning, social and seizure phenotypes. *bioRxiv*. Published online 2020.
18. Jonak CR, Lovelace JW, Ethell IM, Razak KA, Binder DK. Multielectrode array analysis of EEG biomarkers in a mouse model of Fragile X syndrome. *Neurobiol Dis*. 2020;138(November 2019): 104794.
19. Lampert T, Plano A, Austin J, Platt B. On the identification of sleep stages in mouse electroencephalography. *J Neurosci Methods*. 2015;246:52-64.
20. Mondino A, Cavelli M, González J, *et al.* Power and coherence in the EEG of the rat: Impact of behavioral states, cortical area, lateralization and light/dark phases. *Clocks Sleep*. 2020;2(4):536-556.
21. Jiang Z, Huxter JR, Bowyer SA, *et al.* Taini: Maximizing research output whilst improving animals' welfare in neurophysiology experiments. *Sci Rep*. 2017;7(1):1-12.
22. Crunelli V, Lőrincz ML, McCafferty C, *et al.* Clinical and experimental insight into pathophysiology, comorbidity and therapy of absence seizures. *Brain*. 2020(May);143:2341-2368.
23. Bartsch U, Simpkin AJ, Demanuele C, Wamsley E, Marston HM. Jones MW. Distributed slow-wave dynamics during sleep predict memory consolidation and its impairment in schizophrenia. *npj Schizophr*. 2019;5(1):1-11.
24. Nolte G, Bai O, Wheaton L, Mari Z, Vorbach S, Hallett M. Identifying true brain interaction from EEG data using the imaginary part of coherency. *Clin Neurophysiol*. 2004;115: 2292-2307.
25. Den Bakker H, Sidorov MS, Fan Z, *et al.* Abnormal coherence and sleep composition in children with angelman syndrome: A retrospective EEG study. *Mol Autism*. 2018;9(1):1-12.
26. Maris E, Oostenveld R. Nonparametric statistical testing of EEG- and MEG-data. *J Neurosci Methods*. 2007;164(1):177-190.
27. Ingiosi A, Schoch H, Wintler TP, *et al.* Shank3 modulates sleep and expression of circadian transcription factors. *Elife*. 2019;8:1-23.
28. Aceti M, Creson TK, Vaissiere T, *et al.* Syngap1 haploinsufficiency damages a postnatal critical period of pyramidal cell structural maturation linked to cortical circuit assembly. *Biol Psychiatry*. 2015;77(9):805-815.
29. Berryer MH, Chattopadhyaya B, Xing P, *et al.* Decrease of SYNGAP1 in GABAergic cells impairs inhibitory synapse connectivity, synaptic inhibition and cognitive function. *Nat Commun*. 2016;7:1-14.
30. Bosl WJ, Tager-flusberg H, Nelson CA. EEG Analytics for early detection of autism Spectrum disorder : A data-driven approach. *Sci Rep*. 2018:8(1):1-20.
31. Van Luijtelaar ELJM. Spike-wave discharges and sleep spindles in rats. *Acta Neurobiol Exp (Wars)*. 1997;57(2):113-121.
32. Lüthi A. Sleep spindles : Where they Come from, what they do. *Neuroscientist*. 2014;20(3):243-256.
33. Bosl W, Tierney A, Tager-Flusberg H, Nelson C. EEG complexity as a biomarker for autism spectrum disorder risk. *BMC Med*. 2011;9:1-16.
34. Kinney-Lang E, Yoong M, Hunter M, *et al.* Analysis of EEG networks and their correlation with cognitive impairment in preschool children with epilepsy. *Epilepsy Behav*. 2019;90:45-56.
35. Akiyama T, McCoy B, Go CY, *et al.* Focal resection of fast ripples on extraoperative intracranial EEG improves seizure outcome in pediatric epilepsy. *Epilepsia*. 2011;52(10):1802-1811.
36. Cotic M, Zalay OC, Chinvarun Y, Del Campo M, Carlen PL, Bardakjian BL. Mapping the coherence of ictal high frequency oscillations in human extratemporal lobe epilepsy. *Epilepsia*. 2015; 56(3):393-402.
37. Hristova K, Martinez-gonzalez C, Watson TC, *et al.* Medial septal GABAergic neurons reduce seizure duration upon optogenetic closed-loop stimulation. *Brain*. 2021;144(5):1576-1589.
38. Yu T, Wang X, Li Y, *et al.* High-frequency stimulation of anterior nucleus of thalamus desynchronizes epileptic network in humans. *Brain*. 2018;141(9):2631-2643.
39. Dickinson A, Varcin KJ, Sahin M, Nelson CA, Jeste SS. Early patterns of functional brain development associated with autism spectrum disorder in tuberous sclerosis complex. *Autism Res*. 2019; 12(12):1758-1773.
40. Davis PE, Kapur K, Filip-Dhima R, *et al.* Increased electroencephalography connectivity precedes epileptic spasm onset in infants with tuberous sclerosis complex. *Epilepsia*. 2019;60(8):1721-1732.
41. Anderson DE, Madhavan D, Swaminathan A. Global brain network dynamics predict therapeutic responsiveness to cannabidiol treatment for refractory epilepsy. *Brain Commun*. 2020;2(2):1-14.
42. Zelmann R, Lina JM, Schulze-Bonhage A, Gotman J, Jacobs J. Scalp EEG is not a blur: It can see high frequency oscillations although their generators are small. *Brain Topogr*. 2014;27(5):683-704.

43. Petroff OA, Spencer DD, Goncharova II, Zaveri HP. A comparison of the power spectral density of scalp EEG and subjacent electrocorticograms. *Clin Neurophysiol*. 2016;127(2):1108-1112.

44. Hellwig B. A quantitative analysis of the local connectivity between pyramidal neurons in layers 2/3 of the rat visual cortex. *Biol Cybern*. 2000;82(2):111-121.